Am J Clin Exp Urol 2018;6(3):138-148
www.ajceu.us /ISSN:2330-1910/AJCEU0076843

Original Article

Transcriptional changes associated with *in vivo* growth of muscle-invasive bladder cancer cell lines in nude mice

Swathi Ramakrishnan[1], Wendy Huss[1], Barbara Foster[1], Joyce Ohm[2], Jianmin Wang[3], Gissou Azabdaftari[4], Kevin H Eng[3], Anna Woloszynska-Read[1]

Departments of [1]Pharmacology and Therapeutics, [2]Cancer Genetics and Genomics, [3]Bioinformatics and Biostatistics, [4]Pathology, Roswell Park Cancer Institute, Buffalo, NY 14263, USA

Received March 27, 2018; Accepted April 23, 2018; Epub June 15, 2018; Published June 25, 2018

Abstract: Cancer cells set in motion transcriptomic programs allowing for adaptation and growth in immunocompromised mice to form xenografts, a frequently used tool in cancer research. 2D cultures may not be representative of tumors growing in a complex host microenvironment. This can result in different responses to the same agent tested *in vitro* and *in vivo* which impedes the process of developing novel therapeutics. Understanding the transition cells undergo from 2D cell culture to a 3D host microenvironment will help in developing and choosing appropriate models for pre-clinical studies. Our study characterized the transcriptome of a three frequently used muscle-invasive bladder cancer cell lines HT1376, T24 and UM-UC-3 grown in culture and xenografts in nude mice. We found that bladder cancer cells undergo few transcriptomic changes when transitioned from 2D cell culture to xenografts in nude mice. UM-UC-3 cells have the least transcriptomic alterations followed by T24 and HT1376 cells. Respective xenografts cluster with their parental cell lines rather than other xenografts or cell lines. We applied established bladder cancer molecular subtypes to our data and found that UM-UC-3, containing the least transcriptomic alterations, most closely resembled the basal-like molecular subtype of bladder cancer. HT1376 and T24 have mixed basal and luminal molecular signatures. Our studies suggest this subset of bladder cancer cell lines and derived xenografts maintain similar transcriptomic profiles in both 2D culture and 3D xenografts and can be used interchangeably in pre-clinical studies.

Keywords: Bladder cancer, 2D cell culture, xenografts, molecular subtypes, transcriptomics

Introduction

Cancer cells grown in the laboratory have long been used to study mechanisms and signaling pathways in cancer. There is continuing benefit to the use of molecularly classified 2D cell cultures in the era of precision medicine, where tumors in cancer patients are also classified into molecular subtypes [1], because most cell lines retain their oncogenic mutations and hallmarks of the original surgically removed tumor [2]. In addition, cells can be genetically manipulated *in vitro* to understand basic signaling mechanisms and study agents targeting specific molecules [2, 3].

However, 2D cell culture models may not be representative of 3D xenograft tumors growing *in vivo* in mice or human tumors growing in a complex microenvironment [4]. The limitations of 2D cell culture model-based study of human cancers center on the fact that cells within solid tumors growing in a host microenvironment also deal with varying levels of oxygen distribution, nutrients, and at least a subset of immune cells if not the entire immune system. These interactions can fundamentally alter proliferation rates and functional properties of cells within solid tumors compared to cells growing in 2D cell culture [5, 6]. Such alterations of signaling pathways can cause discrepancies in outcomes of therapeutic agents tested in 2D cell culture vs. cells growing as solid tumors in mice or humans [6]. 2D cell culture is also not suitable for studying agents that are pro-drugs and have to be metabolically converted to an active drug molecule [7].

In this scenario, the challenge is to identify appropriate pre-clinical models that maintain the key features of the original tumor properties. Characterizing genetic and epigenetic

alterations in both cell culture and xenograft models addresses the issue of maintaining key tumor features to a large extent. A comprehensive analysis of mutations, copy number variations (CNVs), DNA methylation and gene expression in over 1000 cell lines and 11,000 tumors showed that cell lines and tumors from patients share similar molecular alterations with few of those related to drug resistance/sensitivity [8]. Similarly, the cancer cell line encyclopedia reports mutations, CNVs and gene expression in over 900 cancer cell lines along with pharmacological profiling across 500 cell lines, but bladder cancer is not included in this study [9].

Bladder cancer that has invaded the muscle and spread locally or regionally has survival rates of generally less than two years [10]. Neoadjuvant cisplatin-based chemotherapy and cystectomy are the first line of treatment and have been the only option for these patients over the last three decades. PD-L1 based checkpoint inhibitors have only recently been approved for metastatic urothelial tumors, but these inhibitors show objective response rates in just 20% of patients [11]. With the low rate of therapy discovery and approved therapies working in a small subset of patients, it is critical to choose appropriate pre-clinical models to study advanced bladder cancer and increase the prospects of positive clinical outcomes. Previous studies show a high level of concordance of mutational burden between cell lines and primary tumors in bladder cancer [8] with the identification of molecular signatures from 2D cell cultures that predict cisplatin sensitivity in bladder cancer patients [12]. However, there are no studies to date that investigate the potential alterations occurring in cells transitioning from 2D cell culture to a tumor in a mouse. Therapeutic agents are required to be tested in pre-clinically in laboratory animals before they are introduced in the clinic, therefore it is necessary to understand molecularly the models used in those studies. With this in mind, we studied three muscle-invasive bladder cancer cell lines grown under 2D cell culture and as subcutaneous tumors in nude mice to identify potential transcriptomic alterations between the two growth conditions.

Materials and methods

Cell culture and reagents

HT1376 (ATCC; CRL1472), T24 (ATCC; HTB4) and UM-UC-3 (ATCC; CRL1749) cell lines were used in the study. HT1376 and UM-UC-3 cells were cultured in MEM media (Corning, 10-010) supplemented with non-essential amino acids and T24 cells were cultured in McCoy's media (Corning, 10-050). All the media were supplemented with 10% FBS (Corning, 35-010) and 100 IU Penicillin/100 µg/ml Streptomycin (Corning 30-002) and cultured in 37°C/5% CO_2 incubator. Cell lines were tested for mycoplasma contamination once every two months. Cell counts were obtained using a ViCell counter that uses trypan blue exclusion as a measurement of viable cells. 8×10^4 HT1376 and T24 cells and 1×10^5 UM-UC-3 cells were plated, and cell counts were measured after 96/120 hours using the Vicell counter. Cell doubling time was calculated using the formula: [Duration * Log (2)]/[Log (Final Concentration) - Log (Initial Concentration)].

Cell line-derived xenografts

2×10^6 HT1376 cells, 5×10^6 T24 cells, and 3×10^6 UM-UC-3 cells for each mice were re-suspended in 50:50 HBSS and Matrigel (VWR, 354480) (100 µl total injection volume). The cell-matrigel mix was injected subcutaneously into five nude mice for UM-UC-3 and ten nude mice for T24 and HT1376 each. Tumors were measured twice a week with calipers. Tumor volume was calculated as (L×W×W)/2; where L is the longest axis of the tumor and W is the shortest axis measured in mm. HT1376, T24, and UM-UC-3 tumors were measured for 40 days, 86 days, and 23 days respectively from the time of injection. At the end of the study, mice were humanely euthanized, tumors were harvested, and fresh frozen tissues were stored for RNA extraction or fixed in 10% Neutral Buffered Formalin for paraffin embedding.

RNA extraction and sequencing

RNA extraction was carried out using the ZymoResearch kit. For tumors, RNA was extracted by crushing tumors in liquid nitrogen-cooled mortar and pestle with the the resulting powder suspended in Trizol. For cell lines, cells were rinsed with PBS and Trizol was directly added to the well or plate. The cell and tumor suspensions were incubated in Trizol for 5 minutes at room temperature followed by RNA extraction according to the ZymoResearch protocol. Extracted RNA was analyzed by a bioanalyzer for quality check prior to RNA-sequencing.

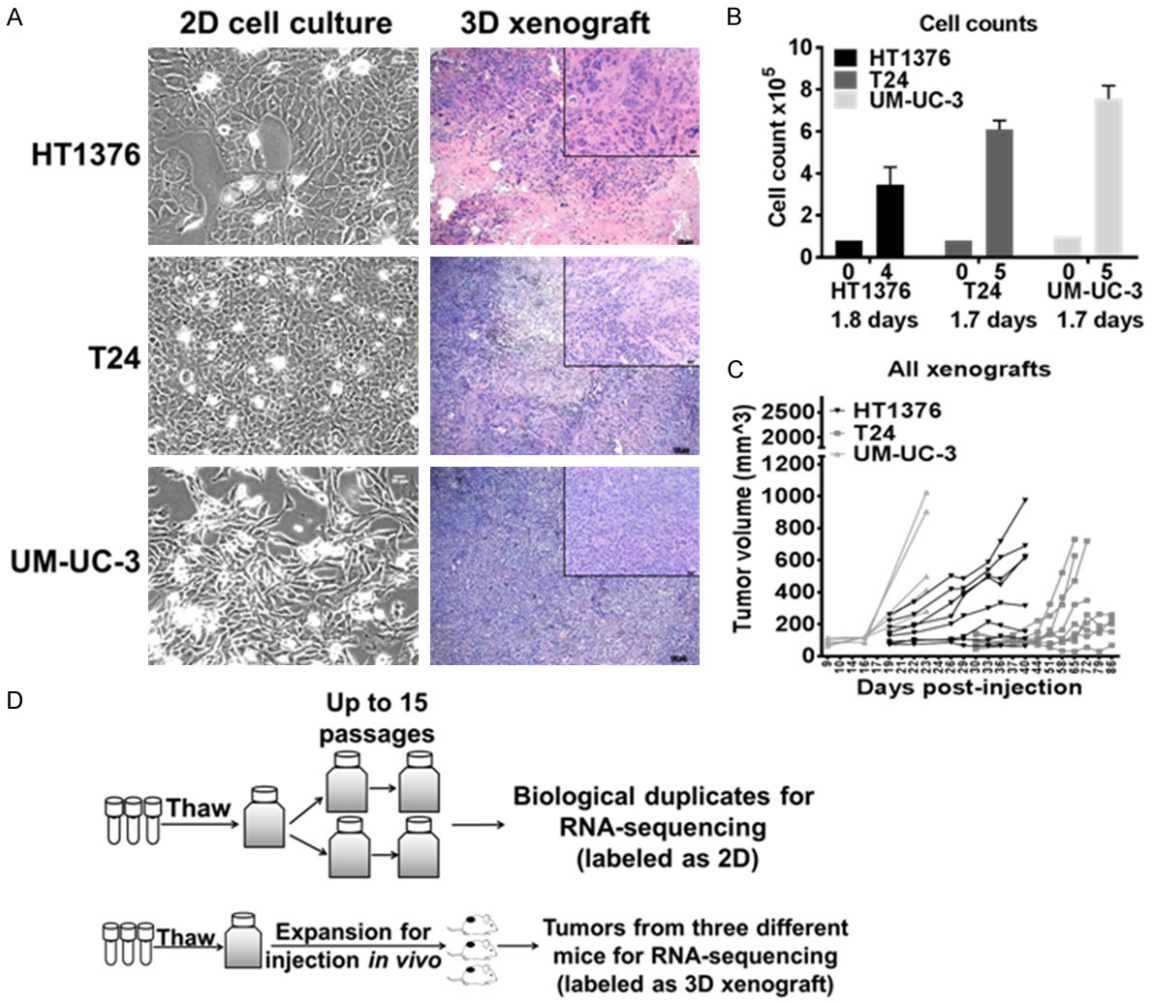

Figure 1. HT1376, T24, and UM-UC-3 bladder cancer cell lines have different morphologies *in vitro* and *in vivo*. A. Left panel represents brightfield images of HT1376, T24 and UM-UC-3 cell lines with distinct morphologies cultured *in vitro*. ___ represents 20 μm. Right panel represents brightfield images of hematoxylin and eosin staining of cell line-derived xenografts that are morphologically different *in vivo*. ___ represents 100 μm in the low power image and 20 μm in the inset. B. 1.2×10^5 HT1376 cells, 0.8×10^5 T24 cells and 1×10^5 UM-UC-3 cells were plated on Day 0. Cell counts were performed at 96 hours (4 days) or 120 hours (5 days) after initial cell plating. The graph shows similar proliferation rate (calculated based on the formula for population doublings in ATCC) between the three cell lines *in vitro*. The Y-axis represents cell counts from biological and technical duplicates. The X-axis represents the different cell lines with 0 being the time of plating and 4/5 being the number of days that the cells were in culture. The error bars represent standard error of means between all the cell counts. C. 2×10^6 HT1376 cells, 5×10^6 T24 cells, and 3×10^6 UMUC3 cells were injected subcutaneously into nude mice. The Y-axis represents the tumor volume measured in mm^3 and X-axis represents the number of days after injection. D. Top panel: Multiple thaws of the different cell lines were cultured for up to 15 passages and two of the passages were analyzed by RNA-sequencing (henceforth known as 2D). Bottom panel: Within the first five passages of thawing, cells were expanded for subcutaneous injection *in vivo*. Tumors from three different mice were analyzed by RNA-sequencing (henceforth known as 3D xenografts).

Bioinformatics and statistical analysis

Accounting for human and mouse host RNA in the 3D xenografts, RNA-seq data were summarized at the gene level as reads per kilobase per million (RPKM). We employed standard ANOVA models to test the main effect of 3D xenografts versus 2D cultures and line specific effects using the Limma and eBayes workflow for RNA-seq [13]. All analyses were performed in the R statistical programming language. Heatmap correlations in **Figure 2A** are all greater than 0.85 (dark grey), the white bins reflect correlations above 0.95. Using established molecular signatures for bladder cancer, we compared differential gene expression across all lines.

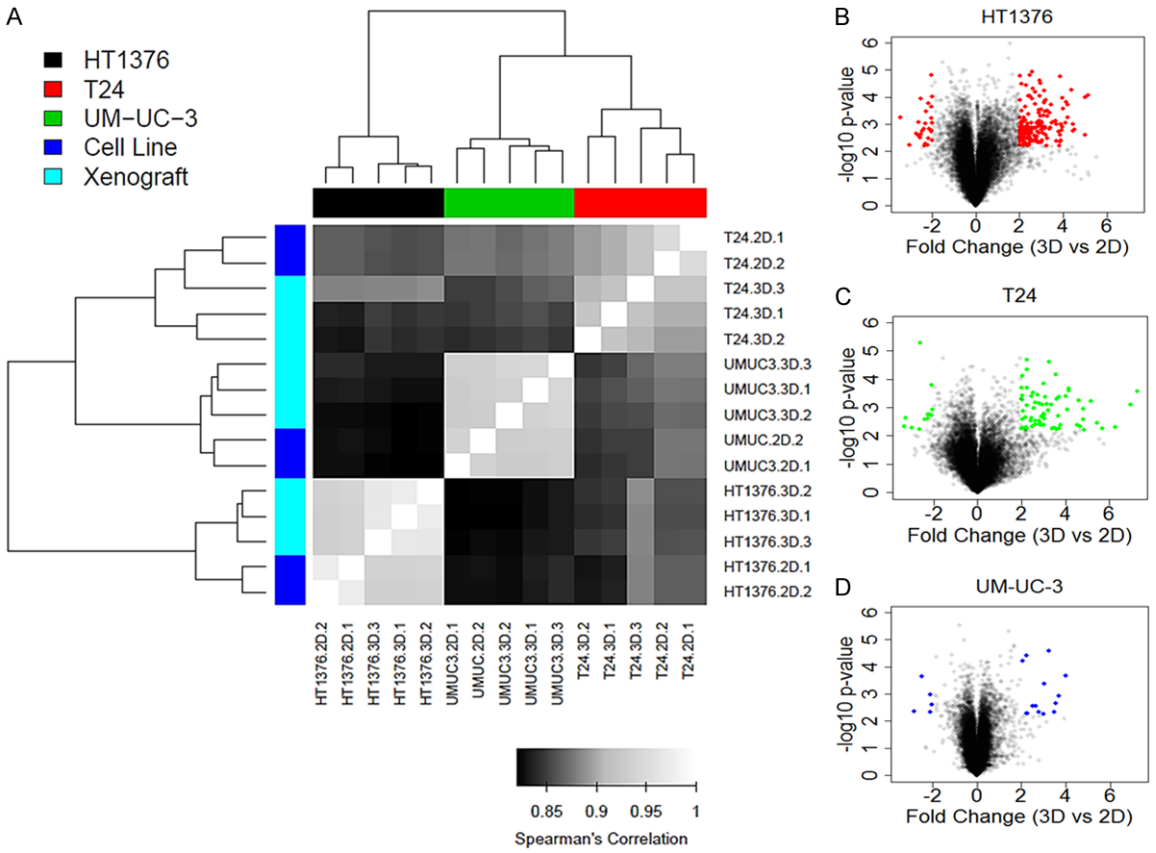

Figure 2. Low variance is observed between cell lines and cell line-derived xenografts from the same parental cells. A. Spearman's correlation based on aggregate statistics of all the genes analyzed by RNA-sequencing show that the cell lines and xenografts from parental cell lines cluster together and are distinct from other cell lines/xenografts. These analyses were based on RNA-sequencing data from biological duplicates for the cell lines (2D) and biological triplicates for the cell line-derived xenograft (3D). B-D. Means of log ratios of RPKM values reveal that there only slight differences between the 2D and 3D models. Colored dots in each plot indicates alterations in gene expression that is greater than 2 fold change ($P<0.05$) in either direction.

Pathway enrichment analysis was performed using Genego by MetaCore from Thomson Reuters. Summary of genes whose descriptions were available on MetaCore are listed in **Tables 1**, **4**, **5**, **6A**, **6B**, **7A** and **7B**.

Results

Bladder cancer cell lines have different morphologies and proliferation rates in vitro and in vivo

Analysis of bladder cancer cell lines shows that genetic alterations including mutations, gene expression, and copy number alterations are similar to those found in patient tumors of bladder cancer [12]. However, there are no studies that evaluate if bladder cancer cells coming from 2D cultures maintain these molecular features after transplantation into a murine host. To investigate this transition process, we used three muscle-invasive bladder cancer cell lines HT1376, T24, and UM-UC-3. *In vitro* (referred to as 2D); HT1376 had a cobblestone-like appearance, T24 had an epithelial-like appearance and UM-UC-3 had fibroblastic appearance (**Figure 1A**). All three cell lines had similar doubling times *in vitro* represented as average number of days ± Standard error of means: 1.8±0.33 days for HT1376 and 1.7±0.06 days for T24 and 1.7±0.06 days for UM-UC-3 cells (**Figure 1B**). These cells were injected subcutaneously into immune-deficient nude mice and xenograft growth was recorded over a period of time. HT1376, T24, and UM-UC-3 derived xenografts (referred to as 3D xenografts) took an average of 40, 65 and 23 days respectively to reach approximately 1000 mm^3 (**Figure 1C**). All three cell line-derived xenografts had similar morphology *in vivo* with more than 80% squamous histology (**Figure 1A**). HT1376 xenografts had

Table 1. List of genes that are altered in all three 3D bladder xenografts

HT1376	T24	UM-UC-3	Count	Gene List
Down	Neutral	Neutral	25	ALPP, ATP6V1B1, COL14A1, CTH, FAM49A, FOLR3, GDPD5, GJA5, GRAMD2, GSTM3, HSD3B1, HTR1D, JAM2, LHX4, MAOA, MAPK4, MGAT3, MTRNR2L8, MYH15, NPTX1, PLSCR4, PRR16, PRUNE2, TNFRSF11B, XAGE2
Neutral	Down	Neutral	10	ABCB1, ABCG2, ADAMTS12, BMF, FAM167A, FLNC, MGST1, NCKAP5, NEGR1, TMEM156
Neutral	Neutral	Down	5	MAR2, CGB5, CGB8, EPAS1, PAPPA
Neutral	Neutral	Up	5	DENND2A, DOCK4, FEZ1, LBH, SNORA33
Neutral	Up	Neutral	51	C10orf10, CAMK2N1, CCAT1, CCDC146, CDH3, CELSR1, COBLL1, CRLF1, CST1, DSP, FAM189A2, FBXO2, FGL2, FRMD4B, GSN, IGSF3, IRF6, ITGB4, JAG2, KRT14, MIR205HG, MUC2, MYLK, MYO1D, NDRG1, NPNT, NT5E, NUPR1, OLFML2A, PLCH2, PVRL1, RASSF6, RNU11, SERPINF1, SH3TC1, SLC6A8, SLITRK6, SLPI, SNORA20, SNORA22, SORL1, SYT8, THY1, TLL2, TNNI2, TNNT3, TRIM29, UBXN10, VCAM1, VIM, WNT7A
Neutral	Up	Up	2	SNORA61, SNORA66
Up	Neutral	Neutral	134	ABLIM1, AIM1, AKR1C2, ALDH3B2, ARRDC3, ATP12A, AXL, B3GNT5, BARX2, BNIPL, C15orf52, C3, CALB1, CALML3, CARD18, CASP14, CCL20, CD70, CDH13, CDSN, CKB, CMPK2, COL1A2, CPE, CRABP2, CSTA, CXCL10, CXCL8, DDIT4, DHRS9, DNER, DSG3, EHF, FCGR3B, FN1, FSCN1, FST, G0S2, GGT6, GSDMC, HCAR3, HDAC9, HEPHL1, HLA-F, HLA-G, HOPX, HR, HSPA6, IFI27, IFI44, IGFBP3, IL1RN, INHBA, IRAK2, ISG15, ITGA5, ITGAM, KLK11, KRT15, KRT16, KRT16P3, KRT4, KRT6A, KRT6B, KRT6C, KRT75, KRT78, KRT79, KYNU, LOC729083, LPAR3, LY6E, MAMDC2, MAP3K5, MFGE8, MMP9, MTSS1, MX2, MXD1, NIPAL4, OAS1, PAG1, PALMD, PARD6G, PDGFC, PDZK1IP1, PFKFB3, PGF, PKP1, PLA2G2F, PLA2G4E, PLAT, PMEPA1, PRDM1, PRKCDBP, PTGS1, PTHLH, RAC2, RHCG, RSAD2, S100A2, S100A7A, SAMD9, SAMD9L, SCEL, SDR16C5, SDR9C7, SERPINA3, SERPINB4, SLC10A6, SLC1A6, SLC22A1, SLC28A3, SNORA53, SPARC, SPINK5, SPNS2, SPRR1A, SPTSSB, THBS1, TM4SF1, TMEM45A, TMPRSS11E, TMPRSS4, TMSB10, TNNT1, TREM1, TRIM22, TYMP, VSNL1, WFDC12, XAF1, ZNF117, ZNF750
Up	Up	Neutral	7	FAT2, HCAR2, IFI44L, KRT17, KRT5, MMP10, TNC
Up	Up	Up	1	H19

Table 2. Pathway enrichment analysis of genes upregulated in HT1376 3D xenografts

#	Enrichment by Process Networks	*p*-value	FDR	In Data	Network Objects from Active Data
1	Inflammation_Amphoterin signaling	5.903E-07	6.789E-05	11	IRAK2, IRAK1/2, ITGAM, MMP-9, Calgranulin C, Calgranulin B, IL-8, IL1RN, PLAT (TPA), S100B, S100P
2	Inflammation_Innate inflammatory response	1.825E-04	1.049E-02	10	IRAK2, IRAK1/2, CCL20, COX-1 (PTGS1), C3b, PLA2, C3a, C3, IL-8, IP10
3	Inflammation_Complement system	5.720E-04	2.193E-02	6	C3b, ITGAM, C3dg, C3a, C3, iC3b
4	Immune response_Innate immune response to RNA viral infection	1.044E-03	2.556E-02	6	IRAK1/2, CCL20, 2'-5'-oligoadenylate synthetase, MxA, IL-8, IP10
5	Proteolysis_ECM remodeling	1.111E-03	2.556E-02	6	Fibronectin, MMP-9, Osteonectin, SERPINA3 (ACT), PLAT (TPA), Kallikrein 3 (PSA)
6	Cell adhesion_Platelet-endothelium-leucocyte interactions	2.774E-03	5.316E-02	8	Fibronectin, LEKTI, ITGAM, MMP-9, PDGF-C, IL-8, Thrombospondin 1, PLAT (TPA)
7	Development_Blood vessel morphogenesis	4.244E-03	6.972E-02	9	Fibronectin, Tissue kallikreins, LEKTI, F263, Galpha(i)-specific EDG GPCRs, PD-ECGF (TdRPase), PLGF, PLAT (TPA), Kallikrein 3 (PSA)
8	Cytoskeleton_Intermediate filaments	5.194E-03	7.467E-02	5	Plakophilin 1, Keratin 6C, Keratin 16, Keratin 6A, Keratin 4
9	Proteolysis_Connective tissue degradation	6.047E-03	7.727E-02	6	Fibronectin, Tissue kallikreins, MMP-9, SERPINA3 (ACT), PLAT (TPA), Kallikrein 3 (PSA)
10	Development_Keratinocyte differentiation	8.365E-03	8.844E-02	4	Caspase-14, Cystatin A, ASK1 (MAP3K5), MAD

Table 3. Functional description of genes downregulated in HT1376 3D xenografts

Gene abbreviation	Function
ALPP	Catalytic enzyme involved in hydrolysis of phosphoric acid monoesters
ATP6V1B1	Involved in the acidification of eukaryotic intracellular organelles
CTH	Converts methionine derived cystathionase into cysteine (essential for glutathione synthesis)
FOLR3	Folate receptor
GDPD5	Involved in glycerol metabolism
GSTM3	Conjugates electrophilic compounds like chemotherapeutic agents to glutathione thereby facilitating removal of these compounds
HSD3B1	Catalyzes the oxidative conversion of steroid precursors
HTR1D	Serotonin receptor
JAM2	Adhesion molecule for a subset of immune cells
LHX4	Transcription factor in pituitary gland development and differentiation
MAOA	Involved in oxidative deamination
XAGE2	Member of the cancer testis antigen family
COL14A1	Involved in development of fine fibrils in collagen fibers
GJA5	Part of gap junction proteins
MAPK4	Belongs to the mitogen-activated protein kinase (MAPK) family
MGAT3	Catalyzes the formation of diacylglycerol
NPTX1	Belongs to the neuronal pentraxin gene family
PRUNE2	Suppresses activity of Ras homolog family member A and oncogenic transformation

Table 4. Pathway enrichment analysis of genes upregulated in T24 3D xenografts

#	Enrichment by Process Networks	*p*-value	FDR	In Data	Network Objects from Active Data
1	Cytoskeleton_Actin filaments	9.635E-07	5.107E-05	8	Myosin I, Troponin I, fast skeletal muscle, Troponin T, cardiac, Troponin T, skeletal, Gelsolin, Beta TnTF, MYLK1, MLCK
2	Cytoskeleton_Intermediate filaments	4.924E-04	1.305E-02	4	Keratin 16, Keratin 14, Vimentin, Desmoplakin
3	Muscle contraction	1.086E-03	1.718E-02	5	Troponin I, fast skeletal muscle, Troponin T, cardiac, Troponin T, skeletal, Beta TnTF, MLCK
4	Cell adhesion_Cadherins	1.297E-03	1.718E-02	5	P-cadherin, M-cadherin, WNT, Prr1, WNT7A
5	Cell adhesion_Amyloid proteins	1.850E-03	1.961E-02	5	Jagged2 (CTF1), Jagged2 (CTF2), WNT, WNT7A, Jagged2
6	Cell adhesion_Cell junctions	6.288E-03	5.554E-02	4	M-cadherin, Vimentin, Prr1, Desmoplakin
7	Development_Neurogenesis_Synaptogenesis	9.075E-03	6.871E-02	4	Synaptotagmin VIII, Synaptotagmin, WNT, WNT7A
8	Development_Skeletal muscle development	2.829E-02	1.874E-01	3	Troponin I, fast skeletal muscle, Troponin T, skeletal, Beta TnTF
9	Development_Ossification and bone remodeling	3.528E-02	2.077E-01	3	WNT, DSPP, WNT7A
10	Signal transduction_WNT signaling	4.761E-02	2.490E-01	3	WNT, Vimentin, WNT7A

greater number of regions with necrosis compared to T24 and UM-UC-3 xenografts (**Figure 1A**). Overall, the three bladder cancer cell lines have similar doubling times with different morphologies *in vitro*. However, *in vivo* all three 3D xenografts develop, at different proliferation rates, subcutaneous tumors with squamous histology.

2D cell cultures and 3D xenografts derived from the same parental line are molecularly more similar to each other than 2D cell cultures and 3D xenografts derived from other cell lines

To determine the changes in gene expression and alteration of signaling pathways when cells adapt from 2D culture to 3D xenografts in mice, we utilized high throughput RNA-sequencing to evaluate gene expression of all three 2D and 3D xenograft bladder cancer models (**Figure 1D**). Spearman correlation analysis showed that HT1376 cells and 3D xenografts were more similar to each other with respect to gene expression than to the T24 or UM-UC-3 models (**Figure 2A**). Similarly, the 3D xenografts derived from T24 and UM-UC-3 clustered closer to their respective parental 2D cell lines than to other 2D cell lines or 3D xenografts (**Figure 2A**). In summary, the 2D cells and 3D xenografts derived from the same parental cell line were more similar to each other with less than 200 genes transcriptionally altered between 2D and

Table 5. Functional description of genes downregulated in T24 3D xenografts

Gene abbreviation	Function
ABCB1 and ABCG2	Involved in multidrug resistance
ADAMTS12	Has proteolytic activity
BMF	Activates apoptosis
FLNC	Filamin proteins that anchor membrane bound protein to actin
MGST1	Conjugates electrophilic compounds like chemotherapeutic agents to glutathione

Table 6A. Functional description of genes downregulated in UM-UC-3 3D xenografts

Gene abbreviation	Function
MAR2	Imprinted retrotransposon that is paternally expressed
CGB5 and CGB8	Member of the glycoprotein hormone beta chain family
EPAS1	Hypoxia inducible factor 2-alpha
PAPPA	Metalloproteinase

Table 6B. Functional description of genes upregulated in UM-UC-3 3D xenografts

Gene abbreviation	Function
DOCK4	Regulates inter-cell adherens junctions
FEZ1	Essential for normal axonal bundling and elongation

3D models. Next, we used t-test analysis to identify gene expression changes that occur within the same set of 2D cells and 3D xenografts. We found that altogether HT1376 had 167, T24 had 71 and UM-UC-3 had 13 genes that were differentially expressed (fold change >2 in either direction, $P<0.05$) in 3D xenografts compared to 2D cells (**Figure 2B-D**). We found 134, 51 and 5 genes to be distinctly upregulated in HT1376, T24 and UM-UC-3 3D xenografts, respectively when compared to their 2D counterparts (**Figure 3A**; **Table 1**). Whereas 25, 10 and 5 genes were distinctly downregulated in HT1376, T24 and UM-UC-3 3D xenografts, respectively when compared to their 2D counterparts (**Figure 3A**; **Table 1**). Gene enrichment analysis of upregulated transcripts in HT1376 3D xenografts were involved in inflammation, proteolysis, cell adhesion, cytoskeletal filaments, and differentiation (**Figure 3B**; **Table 2**). Genes that were downregulated in HT1376 3D xenografts included families of enzymes that catalyze hydrolysis, sulfuration, and conjugation (**Table 3**). In T24 3D xenografts, genes upregulated were involved in cytoskeleton filament development, cell adhesion, skeletal muscle development and Wnt signaling amongst others (**Table 4**). Downregulated genes in T24 3D xenografts included drug efflux genes and an apoptotic regulator, *BMF* (**Table 5**). In UM-UC-3, we observed the least number of gene alterations with upregulation of cell adhesion and downregulation of members of glycoprotein hormone family, hypoxia-inducible factor 2, and a metalloprotease, *PAPPA* (**Table 6A** and **6B**). Additionally, there were 7 and 2 genes commonly upregulated between UM-UC-3 and HT1376/T24 3D xenografts, respectively (**Figure 3A**; **Tables 1**, **7A** and **7B**). Only one gene, H19, a maternally imprinted long non-coding RNA was upregulated in all three 3D xenografts (**Tables 1**, **7A** and **7B**). In conclusion, we show that UM-UC-3 cells grow and form tumors in a subcutaneous nude mouse environment with fewer transcriptomic alterations than HT1376 and T24 3D models. UM-UC-3 3D xenografts have the least number of gene expression changes and a more rapid growth rate suggesting a more aggressive phenotype.

UM-UC-3 cell lines and 3D xenografts have a similar transcriptomic profile as basal molecular subtype of bladder cancer

In gliomas, cell lines or cell-derived xenografts do not accurately represent the genomic aberrations found in glioblastomas from patients [14]. However, in cell lines of bladder, transcriptomic signatures are closely related to patient tumors of bladder cancer and can potentially be used to predict cisplatin sensitivity [12]. Cisplatin sensitivity is also associated with the basal-like molecular subtype of urothelial carcinoma [15]. Therefore, we molecularly classified the 2D cells and 3D xenografts in our study to investigate if these models are representatives of basal or luminal-like bladder tumors by

Table 7A. Functional description of genes commonly upregulated in HT1376 and T24 3D xenografts

Gene abbreviation	Function
FAT2	Tumor suppressor that controls cell proliferation during Drosophila development
HCAR2	Nicotinic acid receptor
IFI44L	Interferon induced protein
KRT17	Type I intermediate chain keratin
KRT5	Type II cytokeratin
MMP10	Breaks down extracellular matrix
TNC	Allows actin-myosin interaction to form tension

Table 7B. Functional description of genes commonly upregulated in HT1376, T24 and UM-UC-3 3D xenografts

Gene abbreviation	Function
H19	Long non-coding RNA located in an imprinted region of chromosome 11 and maternally expressed

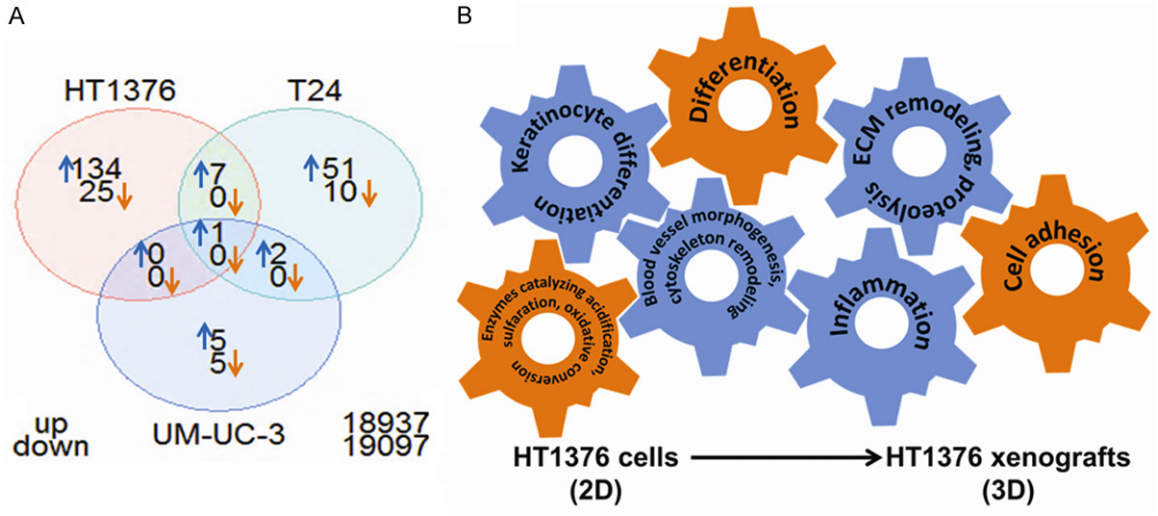

Figure 3. HT1376 subcutaneous tumors have the largest number of gene expression alterations in 3D xenografts compared to T24 and UM-UC-3 tumors. A. The Venn diagram represents the number of genes altered between 2D cells vs. 3D xenograft models as well as between different bladder cancer lines. The numbers on top represent upregulated genes, and the numbers on the bottom represent downregulated genes in 3D xenografts that are common and distinct between cell lines. B. The gears represent the pathways that are altered in HT1376 3D xenografts compared to HT1376 2D cells. Orange color indicates downregulated pathways/gene function and blue color indicates upregulated pathways/gene function.

using previously established signatures [15-18]. Basal-like gene signatures were upregulated in both UM-UC-3 2D cells and 3D xenografts (**Figure 4**). HT1376 2D cells showed upregulation of luminal-like gene signature whereas HT1376 3D xenografts presented with both basal and luminal-like gene expression (**Figure 4**). The differences in HT1376 2D cells and 3D xenografts were not significant and therefore were not included in the previous comparisons of 2D cells and 3D xenografts. Both T24 2D cells and 3D xenografts exhibited gene signatures from basal and luminal-like subtypes of urothelial carcinoma (**Figure 4**). We further analyzed the p53 mRNA levels in all the models. HT1376 and UM-UC-3 models showed increased levels of p53 mRNA in contrast to T24 models that had low levels of p53 mRNA (**Figure 4**). HT1376 and UM-UC-3 harbor missense mutations in p53 whereas T24 has a nonsense mutation in p53 [19]. Overall, these results suggest that UM-UC-3 cells closely resemble the basal-like subtype whereas HT1376 and T24 have mixed basal and luminal signatures.

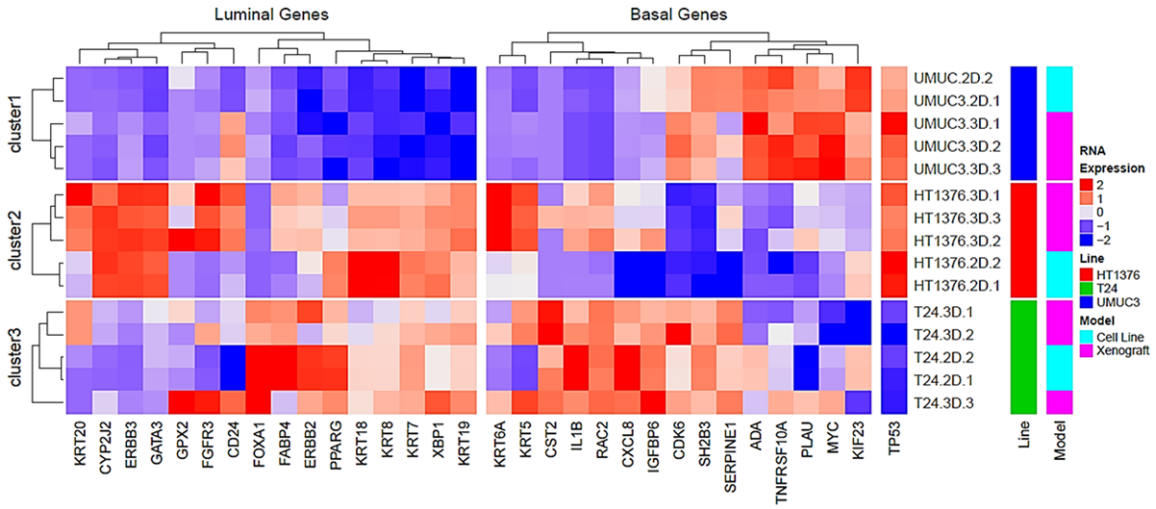

Figure 4. Basal and luminal-like gene signatures observed in HT1376, T24 and UM-UC-3 2D cells as well as 3D xenografts. Differentially expressed genes from previously identified basal and luminal-like subtype of urothelial carcinoma were used to classify the three cell lines as well as cell line-derived xenografts. UM-UC-3 2D and 3D had predominantly a basal-like signature whereas HT1376 and T24 had mixed basal and luminal gene signatures. Expression levels were scaled and centered across all samples for plotting.

Discussion

Our studies show that bladder cancer cells do not undergo dramatic transcriptomic alterations to adapt to and grow in the host microenvironment as 3D xenografts in nude mice. This suggests that HT1376, T24 and UM-UC-3 muscle-invasive bladder cancer cell lines and their derived xenografts are similar pre-clinical models in regards to gene expression alterations associated with their 2D and 3D growth. This is in line with a previous study that showed mutations and gene expression patterns are similar in two bladder tumors, their matching patient-derived xenografts grown in SCID mice and their derived cell lines [20]. Our study and the patient-derived xenograft study [20] used immune-compromised mice to allow human-derived cells to grow as 3D tumors. However, it is important to note that the presence of an immune system might alter the growth and adaptation process [21, 22]. To understand the impact of an intact immune system on gene expression in the 2D to 3D transition future studies should consider utilizing humanized mice. However, we suggest that for developing and testing targeted therapies 2D cells and their 3D xenografts in nude mice are relevant preclinical models. Although we did not observe profound alterations in gene expression, there are other barriers in using these models for pre-clinical studies such as the ability of the drug to reach the tumor. This hypothesis suggests that the use of subcutaneous xenografts in immune compromised mice may be limited to test the efficacy of therapeutic agents to reach its target. Meanwhile, humanized mice with an intact immune system can be used to test agents acting on the immune system for example checkpoint based inhibitors like PD-1 targeted therapies. These considerations are limited to our observations in subcutaneous xenograft models. It might also be worthwhile to develop orthotopic models and models of metastatic disease from these cell lines, and compare their transcriptomic profiles to the parental lines. This will help in selecting appropriate cell lines, xenografts as well as murine backgrounds to study novel therapeutics and develop new treatment approaches.

Our studies also show that the UM-UC-3 cell line closely resembles the basal-like molecular subtype of bladder cancer [15, 16, 18]. Basal-like urothelial tumors are more sensitive to cisplatin-based chemotherapy [15], and UM-UC-3 cells in 2D culture has previously been shown to be cisplatin sensitive [12]. UM-UC-3 xenografts also took the lowest average time to reach 1000 mm^3 and presented with the least transcriptomic alterations from 2D culture to 3D xenografts. This suggests that UM-UC-3 cells present with more aggressive phenotype in xenografts. The previously established cis-

platin sensitivity data [12] and the fact that patients with basal-like molecular subtypes have aggressively growing disease [16, 23] supports the adequate approach to the molecular subtyping of 2D cells and 3D xenografts in our study. HT1376 cells in 2D culture have stronger luminal-like gene signatures however the derived xenografts, as well as T24 models, resemble both the basal and luminal-like subtype. All three cell lines lack functional p53 protein due to nonsense and missense mutations [24]. Therefore, it is unlikely that they belong to the p53-like molecular subtype of bladder cancer that has an activated p53 pathway [16, 18]. Recent developments in analyzing the molecular subtypes of bladder cancer identify additional genetic alterations enriched in the three subtypes [25]. For example: basal-like MIBC tumors are enriched in Rb1 and NFE2L2 mutations whereas luminal-like MIBC tumors are enriched in FGFR3 mutations [25]. Molecular classifications of bladder tumors are still evolving and seem to at least predict sensitivity to neoadjuvant cisplatin-based chemotherapy [12, 15, 16, 25]. Simultaneously, it is important to characterize pre-clinical models including 2D cell culture and 3D xenografts to adequately represent clinical samples along with the molecular subtypes. This will ensure that there exist appropriate models for drug development and therapeutic studies that will potentially have higher chances of success in clinical trials. Our current study shows that 2D culture and 3D xenografts are not associated with radical gene expression changes in three bladder cancer cell lines and can be used for functional studies and pharmacokinetic profiling, respectively, of novel therapeutic agents. In addition, UM-UC-3 2D culture and 3D xenografts represent the basal-like molecular subtype of MIBC and therefore can be used to further understand underlying mechanisms of therapy response and/or resistance specific to basal-like tumors.

Acknowledgements

This work was supported by National Cancer Institute (NCI) grant P30CA016056 involving the use of Roswell Park Cancer Institute's (RPCI) Pathology Network, Genomic, and Clinical Data Network Shared Resources.

Disclosure of conflict of interest

None.

Address correspondence to: Kevin H Eng, Department of Bioinformatics and Biostatistics, Roswell Park Cancer Institute, Buffalo, NY 14263, USA. Tel: 716-845-6504; Fax: 716-849-4860; E-mail: kevin.eng@roswellpark.org; Anna Woloszynska-Read, Department of Pharmacology and Therapeutics, Roswell Park Cancer Institute, Buffalo, NY 14263, USA. Tel: 716-845-8495; Fax: 716-845-1258; E-mail: anna.woloszynska-read@roswellpark.org

References

[1] Pauli C, Hopkins BD, Prandi D, Shaw R, Fedrizzi T, Sboner A, Sailer V, Augello M, Puca L, Rosati R, McNary TJ, Churakova Y, Cheung C, Triscott J, Pisapia D, Rao R, Mosquera JM, Robinson B, Faltas BM, Emerling BE, Gadi VK, Bernard B, Elemento O, Beltran H, Demichelis F, Kemp CJ, Grandori C, Cantley LC and Rubin MA. Personalized *in vitro* and *in vivo* cancer models to guide precision medicine. Cancer Discov 2017; 7: 462-477.

[2] van Staveren WC, Solis DY, Hebrant A, Detours V, Dumont JE and Maenhaut C. Human cancer cell lines: experimental models for cancer cells in situ? For cancer stem cells? Biochim Biophys Acta 2009; 1795: 92-103.

[3] Choi SY, Lin D, Gout PW, Collins CC, Xu Y and Wang Y. Lessons from patient-derived xenografts for better in vitro modeling of human cancer. Adv Drug Deliv Rev 2014; 79-80: 222-237.

[4] Baker BM and Chen CS. Deconstructing the third dimension - how 3D culture microenvironments alter cellular cues. J Cell Sci 2012; 125: 3015-3024.

[5] Weiswald LB, Bellet D and Dangles-Marie V. Spherical cancer models in tumor biology. Neoplasia 2015; 17: 1-15.

[6] Lee JM, Mhawech-Fauceglia P, Lee N, Parsanian LC, Lin YG, Gayther SA and Lawrenson K. A three-dimensional microenvironment alters protein expression and chemosensitivity of epithelial ovarian cancer cells in vitro. Lab Invest 2013; 93: 528-542.

[7] Blumenthal RD and Goldenberg DM. Methods and goals for the use of in vitro and in vivo chemosensitivity testing. Mol Biotechnol 2007; 35: 185-197.

[8] Iorio F, Knijnenburg TA, Vis DJ, Bignell GR, Menden MP, Schubert M, Aben N, Gonçalves E, Barthorpe S, Lightfoot H, Cokelaer T, Greninger P, van Dyk E, Chang H, de Silva H, Heyn H, Deng X, Egan RK, Liu Q, Mironenko T, Mitropoulos X, Richardson L, Wang J, Zhang T, Moran S, Sayols S, Soleimani M, Tamborero D, Lopez-Bigas N, Ross-Macdonald P, Esteller M, Gray NS, Haber DA, Stratton MR, Benes CH, Wessels LFA, Saez-Rodriguez J, McDermott U and Garnett MJ. A landscape of pharmacoge-

nomic interactions in cancer. Cell 2016; 166: 740-754.

[9] Barretina J, Caponigro G, Stransky N, Venkatesan K, Margolin AA, Kim S, Wilson CJ, Lehar J, Kryukov GV, Sonkin D, Reddy A, Liu M, Murray L, Berger MF, Monahan JE, Morais P, Meltzer J, Korejwa A, Jane-Valbuena J, Mapa FA, Thibault J, Bric-Furlong E, Raman P, Shipway A, Engels IH, Cheng J, Yu GK, Yu J, Aspesi P, de Silva M, Jagtap K, Jones MD, Wang L, Hatton C, Palescandolo E, Gupta S, Mahan S, Sougnez C, Onofrio RC, Liefeld T, MacConaill L, Winckler W, Reich M, Li N, Mesirov JP, Gabriel SB, Getz G, Ardlie K, Chan V, Myer VE, Weber BL, Porter J, Warmuth M, Finan P, Harris JL, Meyerson M, Golub TR, Morrissey MP, Sellers WR, Schlegel R and Garraway LA. The cancer cell line encyclopedia enables predictive modelling of anticancer drug sensitivity. Nature 2012; 483: 603-307.

[10] Sonpavde G, Sternberg CN, Rosenberg JE, Hahn NM, Galsky MD and Vogelzang NJ. Second-line systemic therapy and emerging drugs for metastatic transitional-cell carcinoma of the urothelium. Lancet Oncol 2010; 11: 861-870.

[11] Powles T, O'Donnell PH, Massard C, Arkenau HT, Friedlander TW, Hoimes CJ, Lee JL, Ong M, Sridhar SS, Vogelzang NJ, Fishman MN, Zhang J, Srinivas S, Parikh J, Antal J, Jin X, Gupta AK, Ben Y, Hahn NM. Efficacy and safety of durvalumab in locally advanced or metastatic urothelial carcinoma: updated results from a phase 1/2 open-label study. JAMA Oncol 2017; 3: e172411.

[12] Nickerson ML, Witte N, Im KM, Turan S, Owens C, Misner K, Tsang SX, Cai Z, Wu S, Dean M, Costello JC and Theodorescu D. Molecular analysis of urothelial cancer cell lines for modeling tumor biology and drug response. Oncogene 2017; 36: 35-46.

[13] Ritchie ME, Phipson B, Wu D, Hu Y, Law CW, Shi W and Smyth GK. limma powers differential expression analyses for RNA-sequencing and microarray studies. Nucleic Acids Res 2015; 43: e47.

[14] Li A, Walling J, Kotliarov Y, Center A, Steed ME, Ahn SJ, Rosenblum M, Mikkelsen T, Zenklusen JC and Fine HA. Genomic changes and gene expression profiles reveal that established glioma cell lines are poorly representative of primary human gliomas. Mol Cancer Res 2008; 6: 21-30.

[15] Choi W, Porten S, Kim S, Willis D, Plimack ER, Hoffman-Censits J, Roth B, Cheng T, Tran M, Lee IL, Melquist J, Bondaruk J, Majewski T, Zhang S, Pretzsch S, Baggerly K, Siefker-Radtke A, Czerniak B, Dinney CPN and McConkey DJ. Identification of distinct basal and luminal subtypes of muscle-invasive bladder cancer with different sensitivities to frontline chemotherapy. Cancer Cell 2014; 25: 152-165.

[16] Dadhania V, Zhang M, Zhang L, Bondaruk J, Majewski T, Siefker-Radtke A, Guo CC, Dinney C, Cogdell DE, Zhang S, Lee S, Lee JG, Weinstein JN, Baggerly K, McConkey D and Czerniak B. Meta-analysis of the luminal and basal subtypes of bladder cancer and the identification of signature immunohistochemical markers for clinical use. EBioMedicine 2016; 12: 105-117.

[17] Lerner SP, McConkey DJ, Hoadley KA, Chan KS, Kim WY, Radvanyi F, Höglund M and Real FX. Bladder cancer molecular taxonomy: summary from a consensus meeting. Bladder Cancer 2016; 2: 37-47.

[18] Choi W, Czerniak B, Ochoa A, Su X, Siefker-Radtke A, Dinney C and McConkey DJ. Intrinsic basal and luminal subtypes of muscle-invasive bladder cancer. Nat Rev Urol 2014; 11: 400-410.

[19] Forbes SA, Beare D, Boutselakis H, Bamford S, Bindal N, Tate J, Cole CG, Ward S, Dawson E, Ponting L, Stefancsik R, Harsha B, Kok CY, Jia M, Jubb H, Sondka Z, Thompson S, De T and Campbell PJ. COSMIC: somatic cancer genetics at high-resolution. Nucleic Acids Res 2017; 45: D777-D783.

[20] Wei L, Chintala S, Ciamporcero E, Ramakrishnan S, Elbanna M, Wang J, Hu Q, Glenn ST, Murakami M, Liu L, Gomez EC, Sun Y, Conroy J, Miles KM, Malathi K, Ramaiah S, Anbarasu A, Woloszynska-Read A, Johnson CS, Conroy J, Liu S, Morrison CD and Pili R. Genomic profiling is predictive of response to cisplatin treatment but not to PI3K inhibition in bladder cancer patient-derived xenografts. Oncotarget 2016; 7: 76374-76389.

[21] Rongvaux A, Willinger T, Martinek J, Strowig T, Gearty SV, Teichmann LL, Saito Y, Marches F, Halene S, Palucka AK, Manz MG and Flavell RA. Development and function of human innate immune cells in a humanized mouse model. Nat Biotechnol 2014; 32: 364-372.

[22] Zhou Q, Facciponte J, Jin M, Shen Q and Lin Q. Humanized NOD-SCID IL2rg-/- mice as a preclinical model for cancer research and its potential use for individualized cancer therapies. Cancer Lett 2014; 344: 13-19.

[23] McConkey DJ, Choi W, Ochoa A and Dinney CPN. Intrinsic subtypes and bladder cancer metastasis. Asian J Urol 2016; 3: 260-267.

[24] Bouaoun L, Sonkin D, Ardin M, Hollstein M, Byrnes G, Zavadil J and Olivier M. TP53 variations in human cancers: new lessons from the IARC TP53 database and genomics data. Hum Mutat 2016; 37: 865-876.

[25] Choi W, Ochoa A, McConkey DJ, Aine M, Höglund M, Kim WY, Real FX, Kiltie AE, Milsom I, Dyrskjøt L and Lerner SP. Genetic alterations in the molecular subtypes of bladder cancer: illustration in the cancer genome atlas dataset. Eur Urol 2017; 72: 354-365.